Talanta xxx (xxxx) xxx

Contents lists available at ScienceDirect

Talanta

journal homepage: www.elsevier.com/locate/talanta

Au doped poly-thionine and poly-m-Cresol purple: Synthesis and their application in simultaneously electrochemical detection of two lung cancer markers CEA and CYFRA21-1

Huisi Yang [a], Jing Bao [a], Danqun Huo [a,*], Yan Zeng [a], Xianfeng Wang [a], Mickey Samalo [a], Jiaying Zhao [a], Suyi Zhang [a,b,**], Caihong Shen [a,b], Changjun Hou [a,c,***]

[a] Key Laboratory for Biorheological Science and Technology of Ministry of Education, State and Local Joint Engineering Laboratory for Vascular Implants, Bioengineering College of Chongqing University, Chongqing, 400044, PR China
[b] National Engineering Research Center of Solid-State Brewing, Luzhou Laojiao Group Co. Ltd., Luzhou, 646000, PR China
[c] Chongqing Key Laboratory of Bio-perception & Intelligent Information Processing, School of Microelectronics and Communication Engineering, Chongqing University, Chongqing, 400044, PR China

ARTICLE INFO

Keywords:
CYFRA21-1
CEA
Electrochemical biosensor
Simultaneous detection

ABSTRACT

The single tumor antigen does not have enough specificity and sensitivity to meet the accurate diagnostic criteria, and single antigen measurement is often prone to false negative and false positive perceptions. Therefore, simultaneous monitoring of multiple tumor antigens related to precise tumors in serum samples has become an interesting and encouraging analytical method. In this work, we demonstrated an electrochemical biosensor based on multiple signal amplification methods, and simultaneously detect two lung cancer markers, cytokeratin 19 fragment 21-1 (CYFRA21-1) and carcinoembryonic antigen (CEA). Large number of gold nanoparticles distributed on the surface of three-dimensional graphene (3D-G), poly-thionine (pThi) and poly-m-Cresol purple (pMCP) not only provide large number of binding sites for antigen and antibody, but also enhance the electrochemical signal of biosensor and greatly improves the sensitivity of the biosensor. The detection linear range extends from 0.5 to 200 ng/mL, with low detection limits (LOD) of 0.18 ng/mL and 0.31 ng/mL for CYFRA21-1 and CEA, respectively. Overall, this kind of immune-biosensor provides great potential for the simultaneous detection of multiple targets in early clinical diagnosis.

1. Introduction

Lung cancer is one of the most common malignant tumors with substantial morbidity and mortality [1]. It is a great threat to human health and life. Lung cancer ranks first among all causes of cancer death in both women and men throughout the world [2]. In 2018, the death toll was 1.8 million, accounting for 18.4% of the total number of cancer deaths [3]. According to the American Cancer Society, non-small cell lung cancer (NSCLC) accounts for ca. 80% of all new lung cancers, and early detection is one of effective methods to improve the prognosis [4, 5]. Therefore, intensive monitoring strategies for NSCLC patients and the development of appropriate screening methods for the detection of NSCLC biomarkers are urgently needed [6–8].

The basis of immunoassay is the specific recognition of antigen and antibody. Due to its high specificity, immunoassay has become an important tool for quantitative analysis of tumor markers [9–11]. In recent years, the simultaneous detection of multiple tumor markers has become more and more important, because it can improve the accuracy of diagnosis, while reducing sample consumption, detection time and cost [12–14]. Electrochemical immunosensor is an ideal platform for immunoassay to detect and quantify tumor markers accurately and sensitively. It combines the unique advantages of electrochemical

* Corresponding author.
** Corresponding author. Key Laboratory for Biorheological Science and Technology of Ministry of Education, State and Local Joint Engineering Laboratory for Vascular Implants, Bioengineering College of Chongqing University, Chongqing, 400044, PR China.
*** Corresponding author. Key Laboratory for Biorheological Science and Technology of Ministry of Education, State and Local Joint Engineering Laboratory for Vascular Implants, Bioengineering College of Chongqing University, Chongqing, 400044, PR China.
E-mail addresses: huodq@cqu.edu.cn (D. Huo), zhangsy@lzlj.com (S. Zhang), houcj@cqu.edu.cn (C. Hou).

https://doi.org/10.1016/j.talanta.2020.121816
Received 1 July 2020; Received in revised form 20 October 2020; Accepted 23 October 2020
Available online 4 November 2020

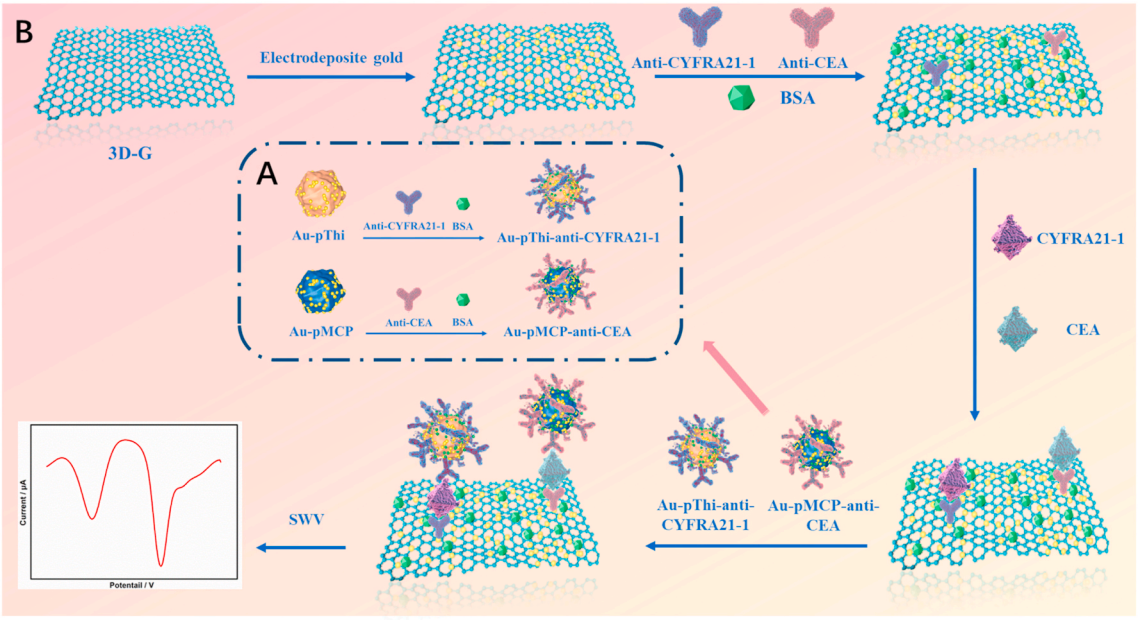

Scheme 1. Schematic illustration of the preparation procedure of immunoprobes **(A)** and the fabrication process of sandwich immunosensor **(B)**.

methods, specific immune recognition reaction and biosensor equipment. In addition, the electrochemical immunosensor has great potential in bedside detection due to its high sensitivity, small sample consumption and low detection cost (POCT) [15].

In principle, simultaneous detection of more biomarkers on one electrode does not facilitate increased sensitivity and lower detection limits [16]. Choosing the right biomarkers can make the detection of NSCLC more accurate. CYFRA21-1 is a soluble fragment of Cytokeratin 19 that is released in the mid-stage of apoptosis [17–19], and it is highly expressed in serum of more than 50% patients with NSCLC [20,21]. CEA is a tumor marker widely existing in the body of various cancer patients, and it has important clinical value in the diagnosis and identification of malignant tumors, the monitoring of patients' condition and the evaluation of therapeutic effects after treatment [22–24].

Electrochemical redox species play a key role in the detection of various biomarkers. In recent years, some fruitful work has been done in the synthesis of new electrochemical redox substances. The Wang et al. [25] study evaluated chip-like GCEs consisting of three parallel-linked GCEs for simultaneous detection of multiple cancer antigens. They combined the advantages of hydrogels and organic nanoparticles to create a sensitive, unlabeled amperometric immunosensor. In this work, sodium alginate was used as the ligand, and Cu (II), Pb (II), Ti (II) were used as dopants to prepare electroactive hydrogels by a one-pot method, which generated three different voltammetric current signals. However, metal ions have some environmental unfriendly problems and desorption problems.

Ma's team [26] used a one-pot method to synthesize four redox species, including three polymeric dye gold composites and a polyaniline gold composite, at room temperature and tested four lung cancer markers simultaneously. Polyaniline derivative is another novel electrochemical redox species, which has great application potential in multi-channel electrochemical immunosensor. With noble metal salt as chemical oxidant, aniline and its derivatives are easy to polymerize. However, in the simultaneous detection of multiple biomarkers on one electrode, the interaction between the molecules will greatly affect the sensitivity and detection limit of the sensor. Thus, for signal amplification, good electron transfer and electrocatalytic capabilities are essential to design new electrochemical redox species to improve the sensitivity of the immunosensor [27,28].

Herein, we used two excellent electrochemical redox species polymers as signal tags and 3D-G/AuNPs nanocomposite with a three-dimensional network porous structure as the substrate to simultaneously detect CYFRA21-1 and CEA. Specifically, we selected two redox species with different peak potentials, and the peak shapes of Thionine (thi) and m-cresol purple (MCP) did not interfere with each other [29]. Also, the polymers of Thi and MCP greatly improve the electrochemical signals of Thi and MCP. The AuNPs on the Au-pThi and Au-pMCP surfaces increase the electron transport on the polymer surface, which increases the detection limit of the sensor. Furthermore, 3D-G large specific surface area can provide large number of binding sites for the modification of other nanomaterials or biomolecules [30–32]. The biomimetic interface of the electrode was constructed by covalent bonding of gold nanoparticles and antibody protein [33]. Modification of anti-CYFRA21-1 and anti-CEA with Au-pThi and Au-pMCP can greatly enhance the electrochemical signals of Thi and MCP, thus enhancing the sensitivity of antigen-antibody binding. This method has high specificity and sensitivity in multiple detection of tumor markers, and has broad application prospects in clinical application.

2. Experimental

2.1. Reagents and materials

Cytokeratin 19 fragment antigen 21-1 (CYFRA21-1), carcinoembryonic antigen (CEA), and corresponding antibodies (anti-CYFRA21-1 and anti-CEA) were purchased from Bioworld Technology Co., Ltd. (Chongqing, China). Chloroauric acid ($HAuCl_4{\cdot}4H_2O$) was acquired from Sinopharm Chemical Reagent Co. Ltd. (China). Graphene oxide (GO) were obtained from Nanjing Xianfeng Nanomaterials Co. (China). Ascorbic acid (AA), dopamine hydrochloride (DA) and uric acid (UA) were obtained from Sigma-Aldrich (Shanghai, China). m-Cresol purple (MCP), thionine (Thi), bovine serum albumin (BSA) and normal human serum were purchased from Solarbio Tech. Co. Ltd. (Beijing, China). All other chemicals are analytical grade and used as received without further purification and all aqueous solutions were freshly prepared with deionized (DI, 18 MΩ cm) water generated by a Millipore Direct-Q Water system.

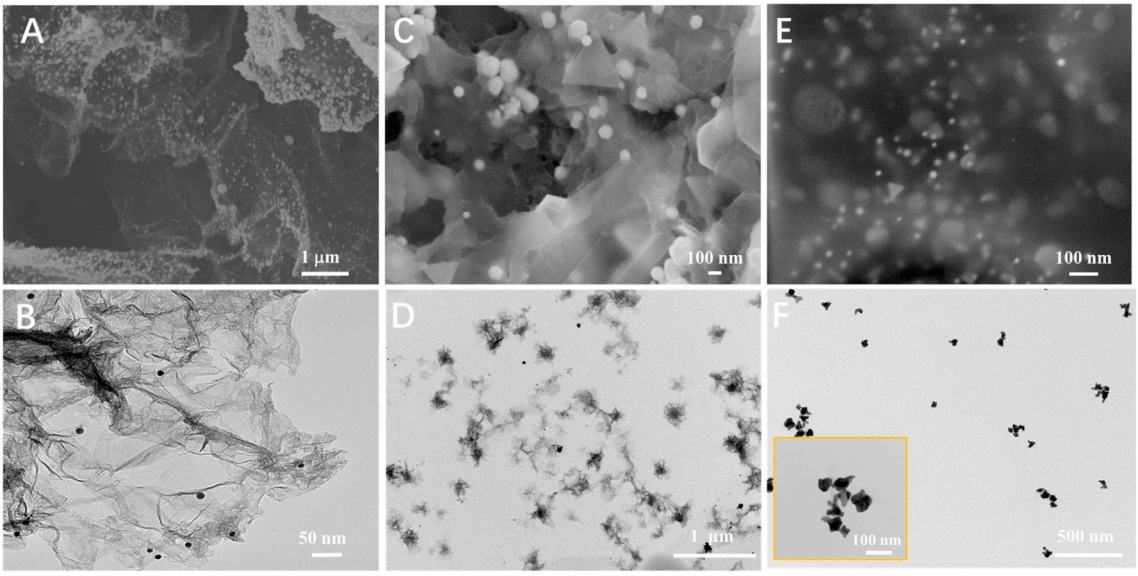

Fig. 1. SEM images of 3D-G/AuNPs **(A)**, Au-pMCP **(C)** and Au-pThi **(E),** TEM images of 3D-G/AuNPs **(B)**, Au-pMCP **(D)** and Au-pThi **(F)**.

2.2. Synthesis of 3D-G, Au-pThi and Au-pMCP

Synthesis of 3D-G: Graphene oxide (GO) was firstly prepared from natural graphite powder by Hummer's method with modification [34]. An aqueous suspension of homogeneous GO (2.5 mg mL^{-1}) was sealed in a Teflon-lined autoclave and heated at 180 °C for 12 h. The obtained 3D-G was washed with DI water for several times before dried by vacuum freeze drying. Finally, 1 mg 3D-G was dissolved in 1 mL 1% chitosan solution to obtain 1 mg mL^{-1} 3D-G solution.

Synthesis of Au-pThi and Au-pMCP: 1 mL of 9.8 mM Thi or MCP ethanol solution was added into 6 mL of 1.72 mM aqueous solution of N, N, *N*-trimethyl-1-dodecanaminium bromide (DTAB) in stirring condition at room temperature to obtain well mixed compound. Then 100 mL of 4% $HAuCl_4$ solution was added to the mixture and stirred for 4 h to allow it to react sufficiently. After the reaction, centrifuge the mixed solution at 16,000 rpm and for 10 min. Washing the sediment by centrifugation with DI water and dispersing it into 1 mL of water [35, 36].

Synthesis of Au-pThi-*anti*-CYFRA21-1 and Au-pMCP-*anti*-CEA: Firstly, 100 mL of antibody solution (1 mg mL^{-1}) was mixed with 100 mL of EDC/NHS (50 mM) solution and stirred slowly overnight. Then, the as-prepared Au-pThi/CEA solution was added into the mixture and stirred for 4 h. In order to eliminate non-specific binding, adding 1 wt% BSA into the mixture as the stirring was maintained for 1 h, then followed by centrifugation for 10 min at 16,000 rpm. Finally, washing the obtained precipitate with DI water for several times and dispersing into 1 mL of PBS (pH = 7) to obtain Au-pThi-*anti*-CYFRA21-1/Au-pMCP-*anti*-CEA.

2.3. Preparation of electrochemical immunosensor

Prior to surface modification, the bare GCE (dia.3 mm) was polished with 1.0 and 0.05 μm alumina slurries and sequentially sonicated in acetone, ethanol and DI water for 1 min, respectively. Then 5 μL of the as-prepared 3D-G suspension (1 mg mL^{-1}) was fixed onto the surface of GCE by drop-casting and dried at room temperature. All the modified electrodes were immersed in mixed solutions (0.01 mol/L Na_2SO_4, 0.01 mol/L H_2SO_4 and 5 mM $HAuCl_4$) and electrodeposited for 200 s at −0.2 V by amperometry (i–t), then were let dry at room temperature. Next, 5 μL of 50 μg/mL of the prepared antibody solution was added to the surface of GCE and reacted at 4 °C for 24 h. After the reaction, the surface of GCE was washed with PBS solution for 2–3 times. Then drop 5 μL of standard antigen solution onto the electrode surface and incubate at room temperature for 60 min. Finally, washing the modified electrode with PBS solution and drying at room temperature. Scheme 1 shows the manufacturing process of the immunosensor.

2.4. Apparatus and electrochemical measurements

The morphology and microstructure of the as-prepared 3D-G/AuNPs were investigated by field-emission scanning electron microscope (FESEM) (FEI Nova 400). Cyclic voltammetry (CV), square wave voltammetry (SWV) and electrochemical impedance spectroscopy (EIS) and other electrochemical measurements were performed on a CHI660E electrochemical workstation (Shanghai Chenhua Instruments Co. Ltd, China). The three electrodes system was employed in the detection system, an Ag/AgCl (3 M KCl) was used as reference electrode, a platinum wire electrode was used as the counter electrode, and the bare or modified glassy carbon electrode was used as the working electrode. CV experiments and EIS investigation were performed in 5 mM $[Fe(CN)_6]^{3-/4-}$ solution containing 0.1 M KCl (1:1 v/v). CV curves were carried out by cycling the potential between scanning from −0.2 V to +0.6 V at a scan rate of 50 mV s^{-1} and EIS investigation was performed with frequencies ranging from 10^{-1} to 10^5 Hz. The square wave voltammetry (SWV) measurements were carried out by scanning from −0.1 V to +0.2 V at amplitude of 50 mV s^{-1} in 0.05 M PBS.

3. Results and discussion

3.1. Characterization of 3D-G/AuNPs and feasibility analysis of immunosensor

Morphology of 3D-G/AuNPs was characterized by SEM and TEM. As shown in Fig. 1A and B, it can be clearly observed that graphene sheets with three-dimensional (3D) spatial structure of are still maintained with many porous and folds. 2D graphene originally has folds and the hydrothermal reduction self-assembly process induces the formation of nano-channels, developing 3D network structure, enabling 3D graphene possess a larger specific surface area than the 2D graphene. It also can be observed that uniformly and densely adhered AuNPs on the surface and pore of 3D-G, as direct electrodeposition method enables to maintain the original morphology and size of AuNPs, allowing more AuNPs to be attached onto the surface and pores of 3D-G. Such arrangement improves conductivity and biocompatibility of the electrode surface and

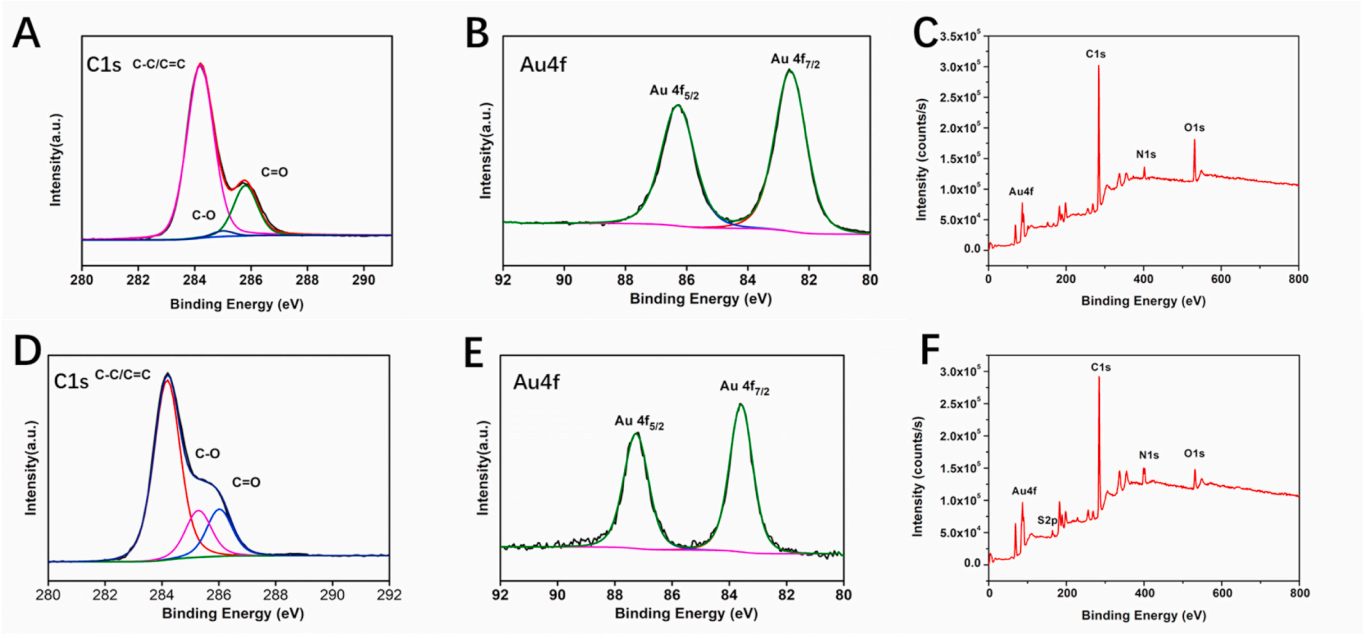

Fig. 2. High resolution XPS spectra of C1s **(A)**, Au4f **(B)** in Au-pMCP samples; XPS survey scan of Au-pMCP **(C)**; High resolution XPS spectra of C1s **(D)**, Au4f **(E)** in Au-pThi samples. XPS survey scan of Au-pThi **(F)**.

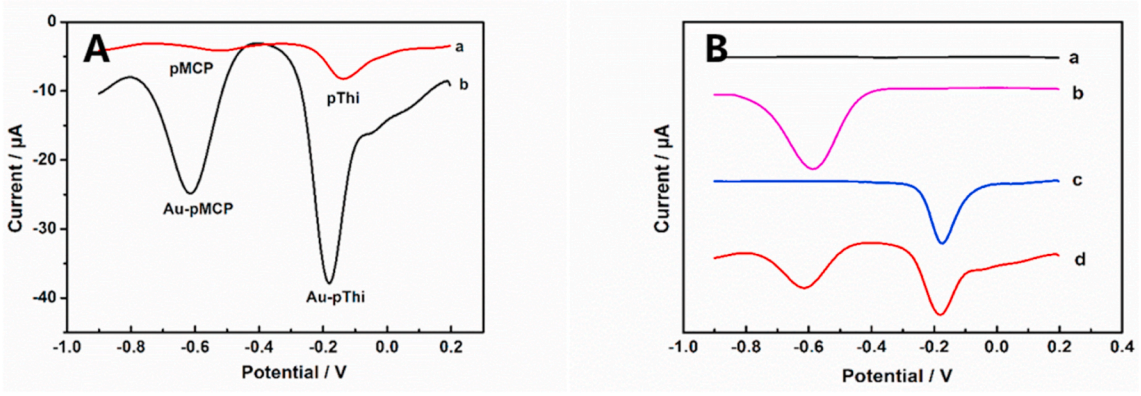

Fig. 3. SWV responses to pMCP and pThi (curve a), and Au-pMCP and Au-pThi (curve b) **(A)** and the cross-reactivity of immunosensors, (a) Blank solution; (b) CEA; (c) CYFRA21-1; (d) CEA and CYFRA21-1 **(B)**.

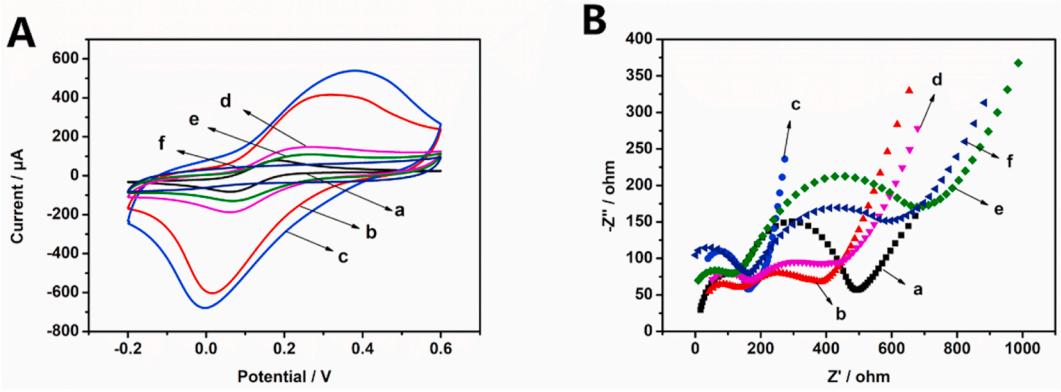

Fig. 4. CV **(A)** and EIS **(B)** obtained for different modified electrodes: (a) bare GCE, (b) 3D-G/GCE, (c)Au/3D-G/GCE, (d)anti-CYFRA21-1/Au/3D-G/GCE, (e) CYFRA21-1/anti-CYFRA21-1/Au/3D-G/GCE, (f)Au-pThi/anti-CYFRA21-1/CYFRA21-1/anti-CYFRA21-1/Au/3D-G/GCE in 5 mM $[Fe(CN)_6]^{3-/4-}$ (1:1) containing 0.1 M KCl solution.

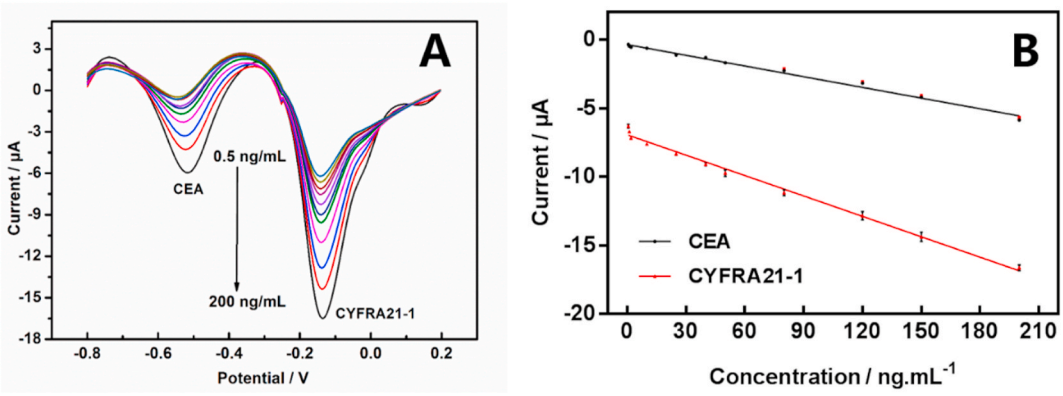

Fig. 5. SWV responses (A) and corresponding calibration curves (B) of the immunosensor for different concentrations of CYFRA21-1 and CEA: 0.5, 1, 2, 10, 25, 30, 40, 50, 80, 120, 150, 200 ng/mL in 0.05 M pH 6.0 PBS. Error bar = RSD (n = 3).

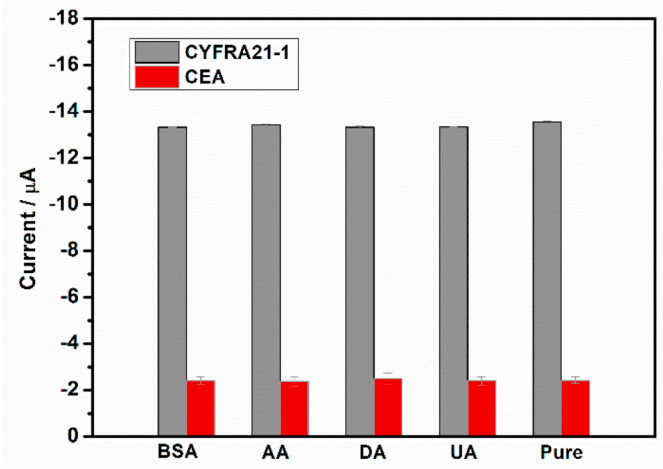

Fig. 6. Interference experiments for 0.2 μg mL^{-1} CYFRA21-1 and CEA, 1 μg mL^{-1} BSA, 1 μg mL^{-1} DA, 1 μg mL^{-1} UA and 1 μg mL^{-1} AA. Error bar = RSD (n = 3).

provides a better biological environment for antibody binding.

SEM and TEM images of signal tags Au-pMCP composite (Fig. 1C and D) and Au-pThi composite (Fig. 1E and F) show that AuNPs interspersed in the composites. Fig. 2C and F shows the complete XPS spectra within the range of 0–800 eV. These overview spectra reveal that C, N, O, and Au atoms are present in the composite. The C 1s (Fig. 2A and D) is attributed to the carbon component in the backbone of the benzene ring, and the N 1s is ascribed to amino or imino groups in the polymers. Besides, the O 1s in Au-pMCP (Fig. 2C) and Au-pThi (Fig. 2F) can be attributed to the carbonyl groups, and the Au 4f (Fig. 2B and E) doublets for Au-pMCP and Au-pThi are consistent with the Au^0 state, indicating that $HAuCl_4$ was reduced to AuNPs. This indicated the successful synthesis of Au-pMCP and Au-pThi polymers.

Compared to the unmodified redox species, Au-pMCP and Au-pThi displayed significant increase electrochemical signal, which greatly increased the detection sensitivity of the proposed immunosensor (Fig. 3A). Such remarkable increase in detection sensitivity was attributed to AuNPs, which provide large number of active sites for covalent immobilization of secondary antibody molecules thus increase the access to antigens and improve electron transfer capability. Taking into consideration the importance of electrochemical performance of two kinds of redox species used in the system, the current response of both redox species to potential need to be explored. The Au-pMCP and Au-pThi exhibited two detachable redox peaks at potential of −0.6 V and −0.2 V, respectively (Fig. 3A curve b). Fig. 3B shows the cross-reactivity of the electrochemical immunosensor. The as-prepared immunosensor was independently incubated with blank solution (curve a), CEA (curve b), CYFRA21-1 (curve c) or CEA and CYFRA21-1 (curve d). An obvious single current response obtained was consistent with the sample containing a single antigen. The immunosensor successfully detected two independent signals in a single run in the mixed solution containing two signals and the peak potentials obtained were consistent with the single detection of the corresponding antigen, indicating that the cross-reactivity between the two antigens can be ignored.

3.2. *Electrochemical characterization of modified electrode*

CV and EIS methods were used to investigate the electrochemical behavior in stepwise construction process (Fig. 4A and B). Fig. 4A shows the peak values obtained vary with each modification applied onto the electrode. Compared with bare GCE (curve a), the electrochemical signals obtained are gradually enhanced after the modification of 3D-G (curve b) and Au/3D-G (curve c), indicating that 3D-G with excellent conductivity and unique porous 3D network can accelerates the electron transfer, and the Au/3D-G can further increase electron transfer rate and enhance the current signal. The peak currents were further decreased after the modifications of anti-CYFRA21-1/Au/3D-G/GCE (curve d), CYFRA21-1/anti-CYFRA21-1/Au/3D-G/GCE (curve e), Au-pThi/anti-CYFRA21-1/CYFRA21-1/anti-CYFRA21-1/Au/3D-G/GCE (curve f), due to the introduction of biological macromolecules fixed via specific

Table 1
Determination of CYFRA21-1 and CEA in serum samples.

Serum Samples	Added antigen (ng/mL)		Found antigen (ng/mL)		RSD/%		Recovery/%	
	CEA	CYFRA21-1	CEA	CYFRA21-1	CEA	CYFRA21-1	CEA	CYFRA21-1
1	150	150	159.28	159.98	−3.2	−2.0	106	107
2	100	100	104.79	92.10	−5.8	−4.0	105	92
3	80	80	82.68	79.67	−7.3	−4.0	103	100
4	50	50	53.54	54.15	−1.6	−2.0	107	108
5	30	30	28.26	28.82	−5.3	−2.0	94	96
6	5	5	4.78	5.17	−8.7	−3.0	96	103

recognition and form layer of organism. Such group of macromolecule complex layer could hinder electron transfer from solution to electrode surface, resulting gradual decrease in peak current of CV along with the modification process.

The results of EIS are shown in Fig. 4B and the variation trend of impedance spectra is consistent with that of CV curves, indicating that the electrochemical immunosensor has been prepared.

3.3. Optimization of experimental conditions

In order to obtain the better detection conditions of this as-fabricated immunosensor, we systematically optimized some affect factors: (i) the incubation time, (ii) the incubation temperature and (iii) the pH value of incubation buffer. The degree of specific reaction between antigen and antibody is closely related to the length of incubation time. As shown in Fig. S1A, the response current increases with increasing incubation time in from 0 up to 60 min. After more than 60 min, the change of response current along with time is feeble, thus 60 min was set as the optimal incubation time in the subsequent experiment.

Since protein antibody is sensitive to temperature change, the effect of incubation temperature was also explored. The proposed immunosensor was incubated in the range temperature from 5 to 65 °C and the response current reaches its maximum at 35 °C, thus 35 °C was selected as the optimized incubation temperature (Fig. S1B).

To achieve optimal performance of the immunosensor, 0.2 μg mL^{-1} of CEA and CYFRA21-1 mixture was incubated in solution with various pH value. As shown in Fig. S1C, the current responses of CEA and CYFRA21-1 were recorded in the solution with pH values range from 3 to 9. The peak current increased with the increasing pH of the detection solution and then tended to decrease in solution with pH higher than 6.0. Hence, pH 6.0 was chosen the optimal pH value of the detection solution.

3.4. Analytical performances of immunosensor for detection of CYFRA21-1 and CEA

AuNPs in Au-pMCP and Au-pThi derivatives and 3D-G/AuNPs nanocomposites on the surface of the immunosensor greatly improve the analytical sensitivity of the immunosensor. The study of analytical performance of immunosensor for detection of CYFRA21-1 and CEA was investigated under the previously mentioned optimal experimental conditions. A good response was achieved as the SWV peak currents of the proposed immunosensor increased gradually with the increasing concentrations of CEA and CYFRA21-1 from 0.5 to 200 ng mL^{-1} (Fig. 5A). The calibration plots show a good linear correlation between the SWV peak currents and the logarithm of CYFRA21-1 and CEA concentrations were obtained (Fig. 5B). The corresponding regression equations are I (μA) = −0.02607 x (ng·mL^{-1}) −0.3543 (n = 11, R^2 = 0.9902) and I (μA) = −0.04957 x (ng·mL^{-1}) −6.932, (n = 11, R^2 = 0.9904) for CEA and CYFRA21-1, respectively. Limits of detection for CEA and CYFRA21-1 were 0.31 ng mL^{-1} and 0.18 ng mL^{-1} (S/N = 3), respectively. The comparison of the linear range and the detection limit between the proposed biosensor and some previously published studies are listed in Table S1. All above results showed that the multi-analytical immunoassay with Au derivative antibody as probe and 3D-G/AuNPs as substrate had a good linear relationship with wide concentration ranges and low detection limits, which have broad application prospects in clinical detection and analysis.

3.5. Specificity, reproducibility stability and cross-reactivity of the electrochemical immunosensor

To further demonstrate the selectivity of the proposed CYFRA21-1 and CEA immunosensor, several potential interfering species in real sample such as bovine serum albumin (BSA), dopamine (DA), uric acid (UA) and ascorbic acid (AA) were investigated. The electrochemical immunosensor was incubated in a series of 0.2 μg mL^{-1} CYFRA21-1 and CEA solutions containing 1 μg mL^{-1} BSA, DA, UA, or AA. Fig. 6 displays that response currents detected from solutions containing interfering species were not significantly different compared to that of solution containing CYFRA21-1 and CEA, suggesting a good selectivity of this designed immunosensor.

The reproducibility of the designed immunosensor was studied by measuring five 0.2 μg mL^{-1} CYFRA21-1 and CEA solutions and the immunosensor regenerated five times under regeneration condition. The result shows that there was no significant difference of peak currents in each measurement with RSD (n = 5) of 5.9% and 8.8% for CYFRA21-1 and CEA, respectively, indicating that the designed immunosensor has a satisfactory reproducibility (Fig. S2).

The stability of the sensor is also an important key factor to be evaluated. The as-prepared immunosensor was stored at 4 °C and measured after 1, 3, 5, 10, 15 and 30 days (Fig. S3). After 30 days of storage, the immunosensor could maintain 93% and 80% of the initial response current of CYFRA21-1 and CEA, respectively, implying acceptable stability performance of immunosensor.

3.6. Performance of electrochemical immunosensor in spiked serum sample

In order to study the practical performance of 3D-G/AuNPs sandwich immunosensor in clinical application, the immunosensor was introduced to a series of serum samples with different concentration of CYFRA21-1 and CEA. The obtained experimental results are listed in Table 1. All the results show that the recoveries were 92.1%–108.4% for CYFRA21-1 and 94.3%–107.0% for CEA with RSD less than 4.0% (n = 3).

4. Conclusion

This work has demonstrated an electrochemical immunosensor for simultaneous detection of CYFRA21-1 and CEA based on multiple nanocomposite-based signal amplification strategy. The 3D-G/AuNPs modified electrode provides a sensitive interface for antigen recognition and Au-pThi and Au-pCMP modification further amplified signals. The developed immunosensor shows a linear detection range of 0.5–200 ng mL^{-1} for both biomarkers with detection limit of 0.18 ng mL^{-1} and 0.31 ng mL^{-1} for CYFRA21-1 and CEA, respectively. In addition, this immunosensor offers high analytical performance in terms of selectivity, reproducibility, and stability. Overall, developed immunosensor shows great potential as a robust tool for simultaneous detection of CYFRA21-1 and CEA.

Credit Author Statement

Huisi Yang: Conceptualization, Methodology, Formal analysis, Writing - original draft. **Jing Bao**: Conceptualization, Formal analysis, Writing - original draft, Writing - review & editing, Supervision. **Yan Zeng**: Conceptualization, Formal analysis, Writing - original draft, Writing - review & editing, Supervision. **Xianfeng Wang**: Conceptualization, Formal analysis, Writing - original draft, Writing - review & editing, Supervision. **Mickey Samalo**: Formal analysis, Writing - review & editing. **Jiaying Zhao**: Formal analysis, Writing - review & editing. **Caihong Shen**: Formal analysis, Writing - review & editing. **Suyi Zhang**: Conceptualization, Methodology, Formal analysis, Writing - review & editing. **Danqun Huo**: Conceptualization, Methodology, Formal analysis, Writing - review & editing. **Changjun Hou**: Conceptualization, Formal analysis, Writing - review & editing, Supervision.

Declaration of competing interest

The authors declare that they have no known competing financial interests or personal relationships that could have appeared to influence

the work reported in this paper.

Acknowledgment

This work was supported by the National Natural Science Foundation of China (NO. 81772290), Graduate Scientific Research and Innovation Foundation of Chongqing, China (Grant No. CYB20070,2020CDCGJ014),Chongqing science and technology commission (CSTC2018jcyjAX0062), Fundamental Research Funds for the Central Universities (2019CDYGZD007),Chongqing Graduate Tutor Team Construction Project and Analytical and Testing Center of Chongqing University for (SEM/XRD/XPS) and the sharing fund of Chongqing University's large equipment.

Appendix A. Supplementary data

Supplementary data to this article can be found online at https://doi.org/10.1016/j.talanta.2020.121816.

References

[1] R.L. Siegel, K.D. Miller, A. Jemal, Cancer statistics, 2019, Ca-Cancer J. Clin. 69 (2019) 7–34.
[2] J. Shi, P.W. Kantoff, R. Wooster, O.C. Farokhzad, Cancer nanomedicine: progress, challenges and opportunities, Nat. Rev. Canc. 17 (2017) 20–37.
[3] F. Bray, J. Ferlay, I. Soerjomataram, R.L. Siegel, L.A. Torre, A. Jemal, Global cancer statistics 2018: GLOBOCAN estimates of incidence and mortality worldwide for 36 cancers in 185 countries, Ca-Cancer J. Clin. 68 (2018) 394–424.
[4] S.L. Topalian, F.S. Hodi, J.R. Brahmer, S.N. Gettinger, D.C. Smith, D.F. McDermott, J.D. Powderly, R.D. Carvajal, J.A. Sosman, M.B. Atkins, P.D. Leming, D.R. Spigel, S. J. Antonia, L. Horn, C.G. Drake, D.M. Pardoll, L. Chen, W.H. Sharfman, R. A. Anders, J.M. Taube, T.L. McMiller, H. Xu, A.J. Korman, M. Jure-Kunkel, S. Agrawal, D. McDonald, G.D. Kollia, A. Gupta, J.M. Wigginton, M. Sznol, Safety, activity, and immune correlates of anti-PD-1 antibody in cancer, N. Engl. J. Med. 366 (2012) 2443–2454.
[5] Z. Hu, X. Chen, Y. Zhao, T. Tian, G. Jin, Y. Shu, Y. Chen, L. Xu, K. Zen, C. Zhang, H. Shen, Serum MicroRNA signatures identified in a genome-wide serum MicroRNA expression profiling predict survival of non-small-cell lung cancer, J. Clin. Oncol. 28 (2010) 1721–1726.
[6] F. Ricci, G. Adornetto, G. Palleschi, A review of experimental aspects of electrochemical immunosensors, Electrochim. Acta 84 (2012) 74–83.
[7] M. Perfezou, A. Turner, A. Merkoci, Cancer detection using nanoparticle-based sensors, Chem. Soc. Rev. 41 (2012) 2606–2622.
[8] Z. Ma, N. Liu, Design of immunoprobes for electrochemical multiplexed tumor marker detection, Expert Rev. Mol. Diagn. 15 (2015) 1075–1083.
[9] J. Shan, Z. Ma, Simultaneous detection of five biomarkers of lung cancer by electrochemical immunoassay, Microchim. Acta 183 (2016) 2889–2897.
[10] Q. Zhu, Y. Chai, R. Yuan, Y. Zhuo, Simultaneous detection of four biomarkers with one sensing surface based on redox probe tagging strategy, Anal. Chim. Acta 800 (2013) 22–28.
[11] D. Feng, L. Li, J. Zhao, Y. Zhang, Simultaneous electrochemical detection of multiple biomarkers using gold nanoparticles decorated multiwall carbon nanotubes as signal enhancers, Anal. Biochem. 482 (2015) 48–54.
[12] L. Wu, X. Qu, Cancer biomarker detection: recent achievements and challenges, Chem. Soc. Rev. 44 (2015) 2963–2997.
[13] M. Ferrari, Cancer nanotechnology: opportunities and challenges, Nat. Rev. Canc. 5 (2005) 161–171.
[14] L. Qi, S. Liu, Y. Jiang, J. Lin, L. Yu, Q. Hu, Simultaneous detection of multiple tumor markers in blood by functional liquid crystal sensors assisted with target-induced dissociation of aptamer, Anal. Chem. 92 (2020) 3867–3873.
[15] J.F. Rusling, C.V. Kumar, J.S. Gutkind, V. Patel, Measurement of biomarker proteins for point-of-care early detection and monitoring of cancer, Analyst 135 (2010) 2496–2511.
[16] Q. Zhu, Y. Chai, Y. Zhuo, R. Yuan, Ultrasensitive simultaneous detection of four biomarkers based on hybridization chain reaction and biotin-streptavidin signal amplification strategy, Biosens. Bioelectron. 68 (2015) 42–48.
[17] R. Malhotra, A.B. Urs, A. Chakravarti, S. Kumar, V.K. Gupta, B. Mahajan, Correlation of Cyfra 21-1 levels in saliva and serum with CK19 mRNA expression in oral squamous cell carcinoma, Tumor Biol. 37 (2016) 9263–9271.
[18] Y. Huang, J. Chan, W. Yan, D. Zang, Q. Qin, A. Deng, Diagnostic accuracy of cytokeratin-19 fragment (CYFRA 21-1) for bladder cancer: a systematic review and meta-analysis, Tumor Biol. 36 (2015) 3137–3145.
[19] H. Wu, P. Wang, J. Yeh, Y. Chen, M. Yen, R. Huang, Y. Tsai, C. Yuan, Serum cytokeratin-19 fragment (Cyfra 21-1) is a prognostic indicator for epithelial ovarian cancer, Taiwan, J. Obstet. Gyne. 53 (2014) 30–34.
[20] N. Kanaji, S. Bandoh, J. Fujita, T. Ishii, T. Ishida, A. Kubo, Compensation of type I and type II cytokeratin pools in lung cancer, Lung Canc. 55 (2007) 295–302.
[21] L. Zhang, D. Liu, L. Li, D. Pu, P. Zhou, Y. Jing, H. Yu, Y. Wang, Y. Zhu, Y. He, Y. Li, S. Zhao, Z. Qiu, W. Li, The important role of circulating CYFRA21-1 in metastasis diagnosis and prognostic value compared with carcinoembryonic antigen and neuron-specific enolase in lung cancer patients, BMC Canc. 17 (2017).
[22] G. Nie, Y. Wang, Y. Tang, D. Zhao, Q. Guo, A graphene quantum dots based electrochemiluminescence immunosensor for carcinoembryonic antigen detection using poly(5-formylindole)/reduced graphene oxide nanocomposite, Biosens. Bioelectron. 101 (2018) 123–128.
[23] S. Benchimol, A. Fuks, S. Jothy, N. Beauchemin, K. Shirota, C.P. Stanners, Carcinoembryonic antigen, a human-tumor marker, functions as an intercellular-adhesion molecule, Cell 57 (1989) 327–334.
[24] S. Hammarstrom, The carcinoembryonic antigen (CEA) family: structures, suggested functions and expression in normal and malignant tissues, Semin. Canc. Biol. 9 (1999) 67–81.
[25] H. Wang, Z. Ma, Simultaneous detection of multiple tumor markers by label-free electrochemical immunoassay using chip-like glass carbon electrodes, Sensor. Actuator. B Chem. 256 (2018) 402–407.
[26] J. Shan, Z. Ma, Simultaneous detection of five biomarkers of lung cancer by electrochemical immunoassay, Microchim. Acta 183 (2016) 2889–2897.
[27] Y. Chang, S. Xie, Y. Chai, Y. Yuan, R. Yuan, 3,4,9,10-Perylenetetracarboxylic acid/o-phenylenediamine nanomaterials as novel redox probes for electrochemical aptasensor systems based on an Fe3O4 magnetic bead as a nonenzymatic catalyst, Chem. Commun. 51 (2015) 7657–7660.
[28] J. Han, Y. Zhuo, Y. Chai, Y. Xiang, R. Yuan, New type of redox nanoprobe: C60 -based nanomaterial and its application in electrochemical immunoassay for doping detection, Anal. Chem. 87 (2015) 1669–1675.
[29] H. Ju, Signal amplification for highly sensitive immunosensing, J. Anal. Testing 1 (2017).
[30] S. Kumar, W. Ahlawat, R. Kumar, N. Dilbaghi, Graphene, carbon nanotubes, zinc oxide and gold as elite nanomaterials for fabrication of biosensors for healthcare, Biosens. Bioelectron. 70 (2015) 498–503.
[31] Y. Song, Y. Luo, C. Zhu, H. Li, D. Du, Y. Lin, Recent advances in electrochemical biosensors based on graphene two-dimensional nanomaterials, Biosens. Bioelectron. 76 (2016) 195–212.
[32] A.T. Lawal, Synthesis and utilisation of graphene for fabrication of electrochemical sensors, Talanta 131 (2015) 424–443.
[33] W. Zhang, Y. Tang, J. Liu, Y. Ma, L. Jiang, W. Huang, F. Huo, D. Tian, An electrochemical sensor for detecting triglyceride based on biomimetic polydopamine and gold nanocomposite, J. Mater. Chem. B 2 (2014) 8490–8495.
[34] J. Ping, Y. Wang, K. Fan, J. Wu, Y. Ying, Direct electrochemical reduction of graphene oxide on ionic liquid doped screen-printed electrode and its electrochemical biosensing application, Biosens. Bioelectron. 28 (2011) 204–209.
[35] J. Shan, Z. Ma, Simultaneous detection of five biomarkers of lung cancer by electrochemical immunoassay, Microchim. Acta 183 (2016) 2889–2897.
[36] F. Jiang, R. Yue, Y. Du, J. Xu, P. Yang, A one-pot 'green' synthesis of Pd-decorated PEDOT nanospheres for nonenzymatic hydrogen peroxide sensing, Biosens. Bioelectron. 44 (2013) 127–131.